Continental Shelf Research 152 (2018) 27–34

Contents lists available at ScienceDirect

Continental Shelf Research

journal homepage: www.elsevier.com/locate/csr

Mean relative sea level rise along the coasts of the China Seas from mid-20th to 21st centuries

Nan Chen[a,b], Guoqi Han[c,*], Jingsong Yang[b,*]

[a] State Key Laboratory of Marine Environmental Science, Xiamen University, Xiamen, China
[b] Second Institute of Oceanography, State Oceanic Administration, Hangzhou, China
[c] Northwest Atlantic Fisheries Centre, Fisheries and Oceans Canada, St. John's, Canada

ARTICLE INFO

Keywords:
Sea level rise
Climate change
Vertical land motion
Satellite altimetry
Global Positioning Systems
Tide-gauge
China Seas

ABSTRACT

Mean relative sea level (MRSL) rise has caused more frequent flooding in many parts of the world. The MRSL rise varies substantially from place to place. Here we use tide-gauge data and satellite measurements to examine past MRSL trends for the coasts of the China Seas. We then combine climate model output and satellite observations to provide MRSL projections in the 21st century. The MRSL trend based on tide-gauge data shows substantial regional variations, from 1 to 5 mm/yr. The vertical land motion (VLM) based on altimetry and tide-gauge (ATG) data indicates large land subsidence at some tide-gauge locations, consistent with the Global Positioning Systems (GPS)-based VLM but different significantly from small uplift estimated by a Glacial Isostatic Adjustment (GIA) model, which suggests other important factors causing the VLM instead of the GIA process. When GPS- or ATG-based VLM estimates are used, the projected MRSL rise between 1986–2005 and 2081–2100 at tide-gauge sites varies from 60 to 130 cm under the Representative Concentration Pathway 8.5 (RCP8.5) scenario of the Intergovernmental Panel on Climate Change (IPCC). Our projections are significantly larger than those of IPCC and other literature, as a result of accounting for the land subsidence derived from observations. Steric and dynamic ocean effects and land-ice melt effects are comparable (about 30 cm each) and do not vary much over the tide-gauge locations. The VLM effect varies from −10 to 60 cm. The projections between 1986–2005 and 2081–2100 under RCP4.5 show a similar spatial distribution to that under RCP8.5, with a smaller amount of rise by 18 cm on average for this region.

1. Introduction

Coastal flooding is often caused by storm surges associated with hurricanes, typhoons and cyclones, in combination with large astronomical tides. Nevertheless, it is the mean sea level rise that is mainly responsible for more frequent coastal flooding around the world in recent decades and can drastically impact coastal communities under a changing climate (UNESCO, 2010; Church et al., 2013). Historical tide-gauge observations indicate that the global mean sea level rise rate is 1.7 ± 0.2 mm/yr over 1900–2009 (Church and White, 2011). Hay et al. (2015) recently found this rate to be 1.2 ± 0.2 mm/yr from 1901 to 1990 and of 3.0 ± 0.7 mm/yr from 1993 to 2010. The global mean sea level rise rate from satellite altimetry is 3.2 ± 0.4 mm/yr over 1993–2009 (Nerem et al., 2010), 3.4 ± 0.4 mm/yr over 1993–2016 (http://sealevel.colorado.edu/content/global-mean-sea-level-time-series-seasonal-signals-removed), and between 2.6 ± 0.4 mm/yr and 2.9 ± 0.4 mm/yr (1993 to mid-2014) after the satellite drift correction being applied (Watson et al., 2015). The Intergovernmental Panel on Climate Change (IPCC) Fifth Assessment Report (AR5) projected likely ranges of global mean sea level rise to be 0.36–0.71 m and 0.52–0.98 m by 2100 (Church et al., 2013) under two Representative Concentration Pathways (RCPs, Moss et al., 2010), i.e. RCP4.5 and RCP8.5, by accounting for thermal expansion from the Fifth Phase of the Climate Modeling Intercomparison Project (CMIP5, Taylor et al., 2012) and the effects of land-ice melt and land water storage and extraction. Recently, increasing efforts have been made towards understanding past sea level trends and projecting future sea level changes on the regional scale (Slangen et al., 2012; 2014). In the present study regional mean sea level is defined as the mean sea level relative to land and therefore depends on vertical land motion (hereafter MRSL). The regional MRSL trend can be significantly different from the global one (Cazenave, 2004). IPCC AR5 regional projections under RCP4.5 have a spatial range from −1.74 to 0.71 m by 2100 relative to 1986–2005. Slangen et al. (2014) found regional variations in sea level change in the world up to 30% above and 50% below the global mean in the 21st century. Han et al. (2015a, 2015b) demonstrated the impacts of accounting for

* Corresponding authors.
E-mail addresses: Guoqi.Han@dfo-mpo.gc.ca (G. Han), jsyang@sio.org.cn (J. Yang).

https://doi.org/10.1016/j.csr.2017.12.002
Received 7 August 2017; Received in revised form 3 November 2017; Accepted 3 December 2017
Available online 06 December 2017

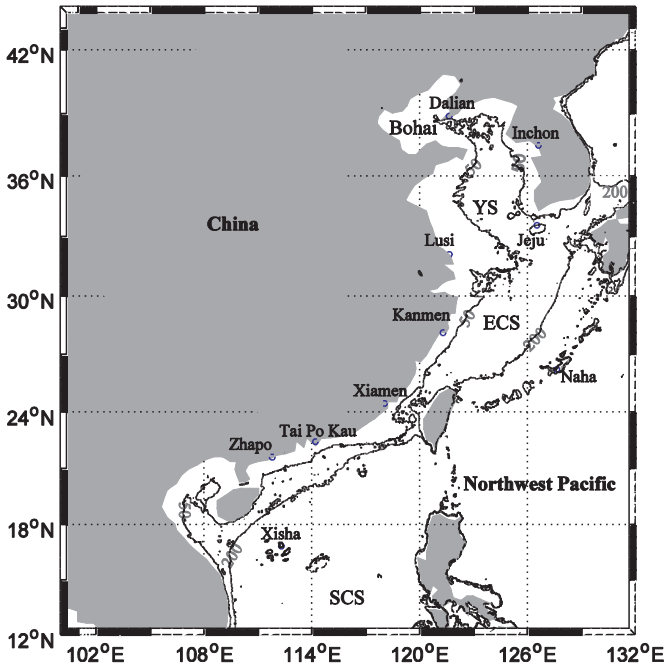

Fig. 1. Map of the study region. Locations of tide gauges are shown. See Table 1 for the data beginning and ending years. YS: Yellow Sea; ECS: East China Sea; SCS: South China Sea.

the vertical land motion caused by other factors (in addition to that by the glacial isostatic adjustment (GIA)) on the 21st-century sea level projections at several North American coastal locations and an East Asian site.

Significant interannual to decadal sea level variability and secular trends exist in the China Seas (Fig. 1) including the South China, East China, Yellow and Bohai Seas (Fang et al., 2006; Cheng and Qi, 2007; Rong et al., 2007; Chang et al., 2008; Han and Huang, 2008, 2009; Cheng et al., 2015), in addition to the seasonal cycle (Han and Huang, 2008, 2009; Cheng et al., 2016b). The interannual and decadal sea level variability is thought to be driven by Pacific Decadal Oscillation (PDO) (e.g. Han and Huang, 2008) and El Niño – Southern Oscillation (ENSO) (e.g. Rong et al., 2007; Chang et al., 2008; Han and Huang, 2009). On the projection side, Slangen et al.'s (2014) and Church et al.'s (2013) regional projections show that sea level rise in the China Seas will be close to the global mean rise. However, their projections do not include non-GIA vertical land motion.

The factors contributing dominantly to global mean sea level change are ocean's thermal expansion and glacier and ice-sheet melt due to the present climate change. The sea level changes due to the above two factors vary from place to place, which can cause notable differences of regional mean sea level change from the global mean sea level change. In addition, the regional sea level change may be associated with many other factors. One factor is the GIA to the last glacial maximum (Peltier, 2004; Slangen et al., 2012). The GIA is the ongoing rise or fall of the land once under and around the great ice sheets which covered much of the Earth's Northern Hemisphere about 20,000 years ago. Another is change in terrestrial water storage such as ground water extraction and reservoir construction (Slangen et al., 2014). The remaining factors include tectonic movement, sediment compaction, and oil and gas extraction. These factors can have large impacts locally, though their impacts are relatively small on the global average. In the China Seas, the land subsidence has notable spatial variations and is mainly caused by overexploitation of groundwater and to some degree engineering activities (Ren, 1994; Lena, 2012; Zhu et al., 2015).

In the present study, we first analyse tide-gauge data, satellite altimetry, and GIA model output (Peltier, 2004) to investigate past (about half century) trends of the MRSL in the China Seas. We then combine an ensemble mean (Slangen et al., 2014) of the CMIP5 climate model output, land-ice model output (Slangen et al., 2014), and GIA model output (Peltier, 2004) to project MRSL rise in the 21st century. In particular, we replace the VLMs of the GIA model with those based on Global Positioning Systems (GPS) or satellite altimetry and tide-gauge data. We will show spatial differences in historical MRSL trends and in projected 21st century rise and to discuss the main contributors to the changes and their spatial differences.

Table 1
Time span of tide-gauge data. See Fig. 1 for tide-gauge locations.

Site	Starting Year	Ending Year
Dalian	1954	2012
Xiamen	1954	2003
Lusi	1969	2012
Tai Po Kau	1963	2011
Kanmen	1959	2012
Xisha	1990	2012
Naha	1967	2012
Jeju	1964	2012
Inchon	1960	2012
Zhapo	1959	2012

2. Data and method

2.1. Tide-gauge data

We have used annual-mean sea level data at selected tide gauge stations (Fig. 1). As of 2012, the time span at all stations is greater than 40 years, except at Xisha where the time span is 23 years only (Table 1). The sea level data are provided by the Permanent Service for the Mean Sea Level (PSMSL, http://www.psmsl.org/).

Annual-mean sea level anomalies at each station are calculated by removing the mean over its data period. We first estimate linear MRSL trends from the sea level anomaly data using a least squares fit. We then use the Durbin-Watson statistic to examine time series of the de-trended sea level anomalies for autocorrelation (Durbin and Watson, 1950; Han et al., 1993, 2015a; Sallenger et al., 2012). If the statistical test indicates autocorrelation at the 95% confidence level, an effective number of degrees of freedom (N_e) is estimated to replace the number of data points (N) in determining the standard error of the estimated trends. N_e can be estimated using the lag-1 autocorrelation as

$$N_e = N(1-r)/(1+r) \quad (1)$$

where r is the lag-1 autocorrelation coefficient from a first-order autoregressive model fitted to the de-trended sea level anomalies (Sallenger et al., 2012). The effect of serial correlation is the reduction of the number of degrees of freedom, amplifying the standard error of estimated sea level trends.

2.2. Satellite altimetry data

Satellite altimetry, despite its relatively short data record (~ 20 years), has played an important role in monitoring and understanding absolute or geocentric sea level changes (i.e., relative to the Earth's centre of mass) on both global and regional scales. The geocentric sea level rate as derived from satellite altimetry is not influenced by local land motion.

We have used weekly sea surface height anomalies from AVISO (Archiving, Validation and Interpretation of Satellites Oceanographic data) (http://www.aviso.oceanobs.com/en/altimetry/index.html) for 1993–2012, an objectively mapped product of TOPEX/Poseidon, Jason-1, Jason-2, ERS-1, ERS-2, Geosat-Follow-on and Envisat altimeter data, with a 1/3° Mercator projection grid (Ducet at al., 2000). AVISO data were corrected for wet troposphere, dry troposphere, and ionosphere

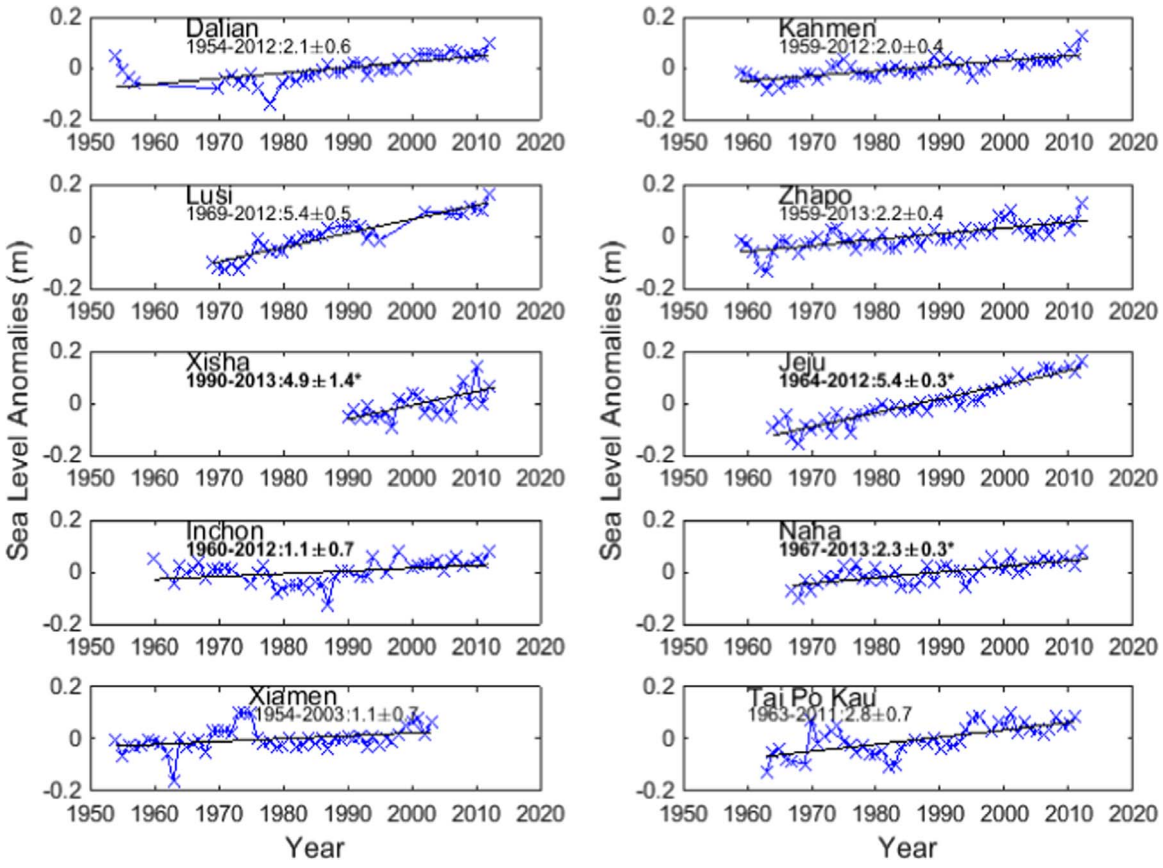

Fig. 2. Annual-mean RSLs at tide-gauge stations and linear trends (± one standard error) for the entire data period. The star indicates that there is autocorrelation (at the 95% confidence level) in the annual-mean RSLs and therefore the standard error is calculated based on the effective number of degrees of freedom (See Section 2.1). See Fig. 1 for locations.

effects, inverted-barometer responses, dynamic responses to high-frequency pressure and wind forcing, and sea state bias. They were also corrected for ocean, solid earth and pole tides. Linear trends and associated standard errors are derived from the altimetric data using a least squares fit as described in Section 2.1, with the effects of autocorrelation of altimetric data on the errors of the trends accounted for.

The AVISO product has found wide applications in the deep ocean (Fu and Cazenave, 2001). However, altimetric data are not available within tens of kilometres from coast and their quality may be poor nearshore (Vignudelli et al., 2011). That being said, it has been shown (Han and Huang, 2008, 2009) that altimetric data can be used to study annual and longer-term sea level variations in the China Seas. A recent study (Wöppelmann and Marcos, 2016) found that satellite altimetry can capture monthly coastal sea levels reasonably well at most of the tide gauge locations worldwide.

2.3. *Peltier's (2004) glacial isostatic adjustment model*

We use the GIA (ICE-5G, VM2) results of Peltier's (2004) global model. The model output includes the present-day VLM and the net MRSL change associated with the GIA in a 1° longitude by 1° latitude grid. At tide-gauge stations, we use the Peltier's model result provided by the PSMSL, (http://www.psmsl.org/). There are other global GIA models, e.g., the Austrian National University (ANU) model (Lambeck et al., 1998). Since the two models produce very close results in the study region, we choose to use the Peltier's model. In addition, we use VLM estimates from GPS data based on literature, where available.

2.4. *Estimation of vertical land motion*

Following Han et al. (2014), we infer the rate of the vertical land motion (VLM, positive upward) by subtracting the sea level trend derived from altimetric data from that derived from the tide-gauge data (hereafter referred to as the ATG VLM) during the same period. Note that the ATG estimates include any VLM caused by other factors, in addition to the GIA. The altimetric rate at a tide-gauge location is obtained using the nearest-neighbour method from the 1/3° by 1/3° gridded data.

The standard error associated with the ATG VLM is estimated as the root-sum-square of the standard errors associated with the altimetric and tide-gauge rates by assuming these errors are uncorrelated. The grid resolution effect could cause additional errors that are difficult to estimate and thus not included in the standard errors.

2.5. *Sea level projections*

We have used Slangen et al.'s (2014) projection components between 1986–2005 and 2081–2100, under IPCC AR5 medium (RCP4.5) and high (RCP8.5) emission scenarios. We include an oceanographic component (an ensemble mean of sea levels from 21 CMIP5 climate models), contribution of land-ice melt, and Peltier's (2004) GIA model output. The oceanographic component is provided on a 1° by 1° grid. The land-ice contribution includes the effects of glaciers, ice caps, Greenland Ice Sheet, and Antarctic Ice Sheet. The contributions by oceanographic change and land-ice melt are extrapolated onto tide-gauge locations using the nearest-neighbour method. We note that there could be errors due to extrapolation and grid resolution effect, which are not accounted for in our study.

In the present study, the GPS- or ATG-based VLMs are used to replace the model GIA VLMs at tide-gauge stations, which can account for non-GIA VLM effects, such as land-ice melt, ground water extraction, sediment compaction and tectonic movement. The standard errors for

total projections are calculated as the root-sum-square of the errors in the ocean, land-ice and GIA components provided in Slangen et al. (2014), as well as the standard errors in the GPS or ATG VLM described in Section 2.4, by assuming these errors are uncorrelated.

Because the GPS- or ATG-based VLM includes the VLM associated with the land-ice melt over the data-collection period, the present approach double counts the VLMs associated with land-ice melt. Nevertheless, the VLM rate associated with the present land–ice melt is estimated to be −0.3–0.1 mm/yr in the study region, which translates to −3–1 cm for the projection period of 95 years. In addition, the present approach implicitly assumes that the VLM rate except for that associated with land-ice melt is invariable during the study period. This assumption may not be appropriate, except for the VLM rate associated with the GIA process (See Section 4 for further discussion).

3. Past trends

3.1. Past sea level trends from tide-gauge data

There are significant spatial changes in the MRSL trends (Fig. 2) in the study region. The MRSL rates over the entire data periods vary from 1 mm/yr to 5 mm/yr at the tide-gauge sites. They are all significantly different from zero at the 95% confidence level, except at Xiamen and Inchon. At some of the sites, there is autocorrelation (at the 95% confidence level) in the annual-mean RSLs (indicated by stars in Fig. 2) and therefore the standard error is calculated based on the effective number of degrees of freedom. The rate along the continental coastline is relatively small, except at Lusi where the rate is as high as 5.4 mm/yr. High rates of about 5 mm/yr are seen in the two island sites of Xisha (in the South China Sea) and Jeju (in the East China Sea).

There are indications of substantial interannual and decadal variations (Fig. 2), with annual-mean RSLs deviating from the fitted straight line. For example, there are positive and negative deviations at Tai Po Kau in the early 1970s and in the early 1980s, respectively. Previous studies have indicated the18.6-yr nodal cycle, with amplitude of 1–3 cm along the Chinese coast (Su and Yuan, 2005; Feng et al., 2015). The coastal sea level variations may also be associated with the Pacific Decadal Oscillation (e.g. Han and Huang, 2008; Strassburg et al., 2015) and ENSO (e.g. Rong et al., 2007; Chang et al., 2008; Han and Huang, 2009; Cheng et al., 2016a). Nevertheless, a detailed study on the interannual and decadal variations is beyond the scope of the present paper, but their impacts on the uncertainty of the secular trend estimates are quantified by using the method described in Section 2.1.

Long-term MRSL trends in the past are a combination of contributions by ocean warming and dynamic adjustment, land-ice melt, and VLM. At the tide-gauge locations in the China Seas, the ocean warming and dynamic adjustment contributes 0–1 mm/yr over the period from 1970 to 2010, according to the monthly Simple Data Assimilation Model (SODA, Carton and Giese, 2008) sea level product (Fig. 3). The SODA product has a 0.5° by 0.5° grid. Satellite observations show that the global sea-level rise due to the land ice melt over 1993–2010 has accelerated. To reasonably represent the linear sea level rise over 1970–2010, we use linear rates over 1971–2010 for glaciers, and over 1992–2001 for Antarctic and Greenland ice sheets provided in Church et al. (2013). As such, the linear rate of the global sea-level rise as a result of the land-ice melt is estimated to be 0.8 mm/yr. Since our study region is in the far field, the fingerprint of the land-ice melt is slightly larger (about 1.2 times) than the global average, i.e., 1 mm/yr. The combined contribution from the ocean warming and dynamics and the land-ice melt varies spatially from 1 to 2 mm/yr, much smaller than the variation of 1–6 mm/yr in tide-gauge data. Therefore, the large regional differences in the MRSL trends as observed from tide-gauge data must be contributed by VLM, which is investigated in the next subsection.

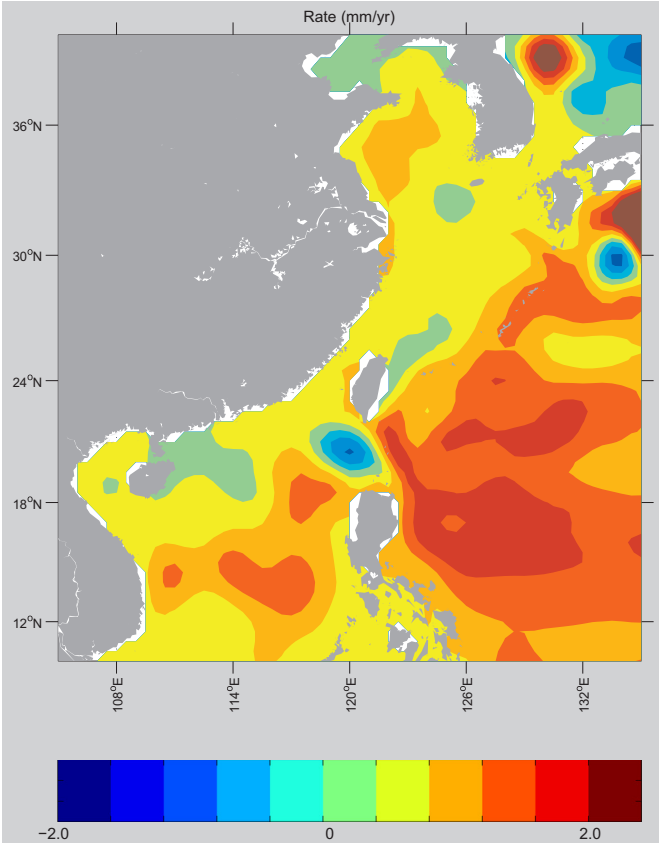

Fig. 3. Sea level rise rate (mm/yr) based on the SODA output (Carton and Giese, 2008) over 1970–2010.

3.2. Vertical land motion

Over the Northwest Pacific, Peltier's (2014) model indicates that the GIA process results in small land uplift (Fig. 4a and Fig. 5). Our study region is far from the major centres of the last glacial maximum, the central North America and the Scandinavia, therefore the GIA impact is small. The GIA affects the MRSL at a location from two aspects: VLM and sea surface topography itself. The latter is associated with the water redistribution in response to the movement of the solid earth and has smaller magnitude than the former. Because sea level is gravitationally attracted to land, high land induces an increase (small) to the local relative sea level. A positive (negative) VLM contributes negatively (positively) to relative sea level rise at that location. As a result, the net GIA effect in the study region is MRSL fall with magnitude smaller than that of the GIA VLM (Fig. 4b).

We have derived the geocentric sea level change rate in the study region from the altimetry data for 1993–2012 (Fig. 6). The geocentric sea level increases at 0–2 mm/yr in most of the study region over the past two decades, except east of the Philippines. It is worthwhile pointing out that the derived linear trend is subject to large uncertainty, due to the short time span of only about 20 years.

The VLM derived from the ATG over 1993–2012 is largely negative (−5 to −1 mm/yr) except at Inchon and Zhapo (Fig. 5), which is a large deviation from estimates by Peltier's GIA model. Note that negative VLM means land subsidence. The large difference between the ATG estimate and the GIA model suggests other factors instead of the GIA are responsible for the VLM at the study locations. Possible factors include ground water extraction and sediment compaction (Church et al., 2013). Jeju is a large island and groundwater is the only source of freshwater (Choi, 2012). Exploitation of groundwater has been extensive for agricultural, industrial and domestic consumption. Thus the major factor for the large land subsidence at Jeju is ground water

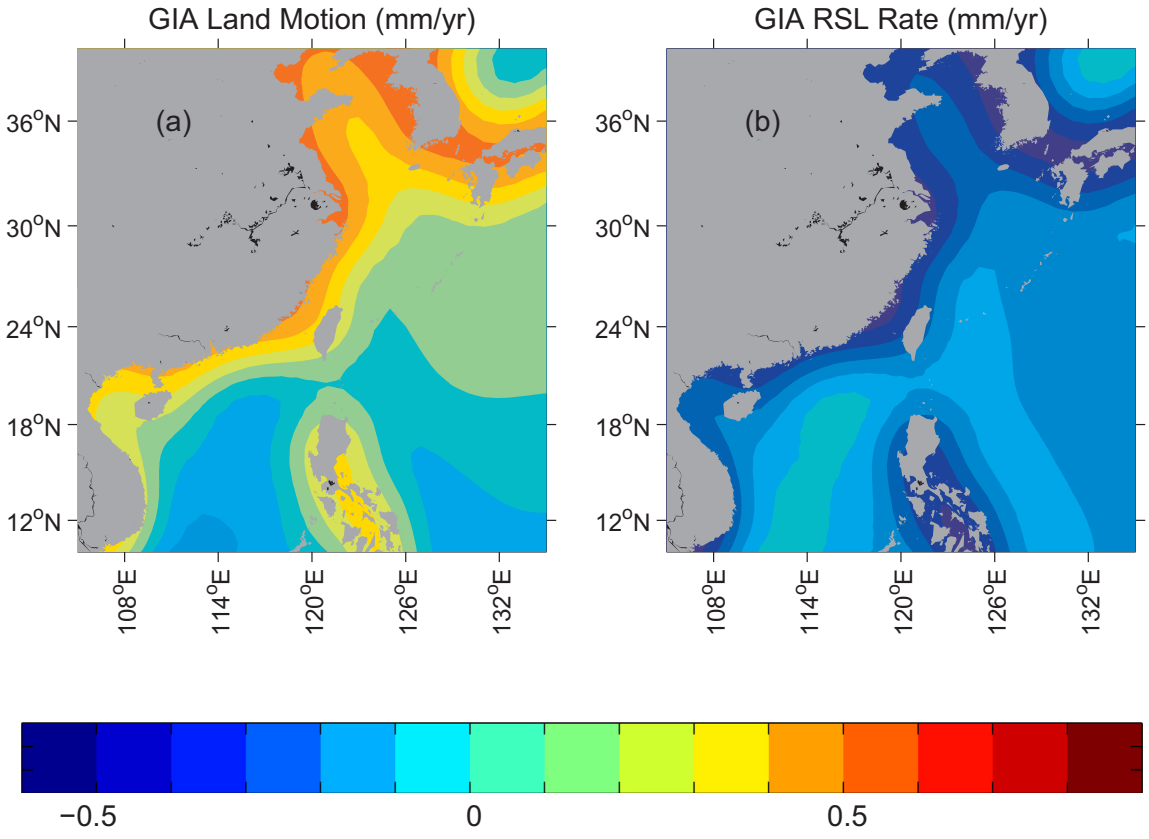

Fig. 4. (a) VLM Rate due to GIA from Peltier's (2004) model. (b) Rate of the MRSL change due to GIA from Peltier's (2004) model.

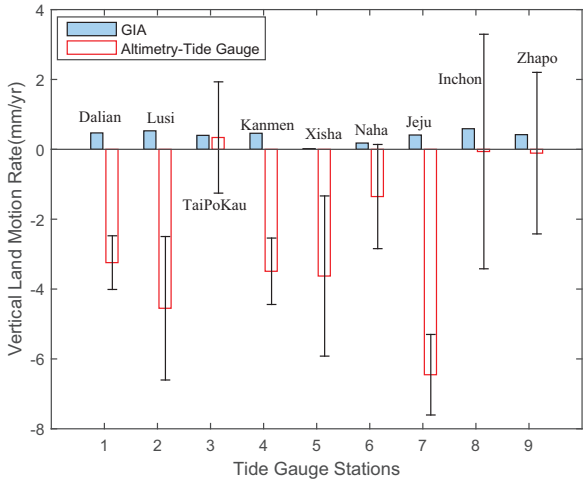

Fig. 5. VLM rate (mm/yr) at tide-gauge stations. The GIA model value is the average over the period 250 years before and after the present. The value of altimetry - tide-gauge (± one standard error, black vertical line) is for 1993–2012.

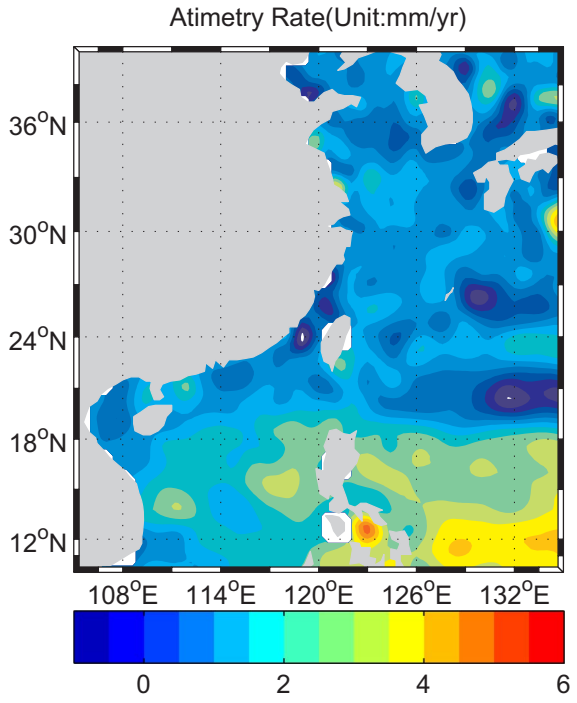

Fig. 6. Geocentric sea level rate from altimetry data for the period from 1993 to 2012.

extraction (Choi, 2012; Han et al., 2015b). Lusi is located in the Yangtze Delta, which is one of the regions in China with severe land subsidence (Ren, 1994; Lena, 2012). The land subsidence in the vicinity of Lusi, with superficial layers of loose sediment geologically, is mainly caused by overexploitation of groundwater and to some degree engineering and construction activities (Zhu et al., 2015). The ATG VLM estimates are subject to large uncertainties, as shown in Fig. 5. The uncertainties may be attributed to errors associated with altimetry data, from measurements, environmental corrections, to extrapolation. They may also be attributed to decadal variability and the 18.6-yr nodal cycle. Nevertheless, the ATG VLM estimates are significantly different from zero at the 95% confidence level at Dalian, Jeju, Kanmen, and Lusi.

The VLM estimates from ATG are compared with those from GPS data at three stations (Table 2). The GPS VLM value is from Chen et al. (2010) (an average at two nearby sites for Tai Po Kau), from Liu (2013) for Kanmen, and from Bouin and Woppelmann (2010) for Naha. Note

Table 2
Comparison of VLM rates (mm/yr) at three tide-gauge stations: ATG versus GPS. The GPS value is from Chen et al. (2010) (an average at two nearby sites for Tai Po Kau, from Liu (2013) for Kanmen, and from Bouin and Woppelmann (2010) for Naha.

Station	ATG	GPS
Tai Po Kau	0.4 ± 1.3	0.4 ± 0.7
Kanmen	−3.5 ± 0.9	−2.3
Naha	−1.3 ± 1.5	−0.1 ± 2.3
Mean	−1.5	−0.7
Mean Difference	−0.8	N/A
RMS Difference	1.0	N/A

that the ATG values are for the period from 1993 to 2012 and the GPS values are for much shorter periods (from 2006 to 2007 for Tai Po Kau (Liu, 2013), but information on the exact period is unavailable for the other two stations). Since the GPS data have short duration the GPS VLM estimates may be subject to large uncertainties too. The ATG estimates at the three stations have an average VLM of −1.5 mm/yr, qualitatively (in terms of the direction of VLM) consistent with the GPS average of −0.7 mm/yr. In contrast, the GIA-model VLMs have an average value of 0.4 mm/yr, inconsistent with the direction of the GPS VLM. Additionally, the ATG VLM is able to approximately capture the spatial difference in the GPS VLM among the three stations, while the GIA VLM is not. The mean bias of −0.8 mm/yr in the present study region is comparable to that in Atlantic Canada (Han et al., 2014). The root mean square (RMS) difference between the ATG and GPS VLMs is 1.0 mm/yr. In the following section we will use the GPS VLM at Kanmen, Tai Po Kau and Naha and the ATG VLM for the other stations for MRSL projections.

4. Projections of sea level rise

Sea level projections from Slangen et al. (2014) are shown in Fig. 7 for the period from 1986–2005 to 2081-2010. Two emission scenarios, RCP4.5 and RCP8.5, are considered. The MRSL rise under RCP8.5 varies from 50 to 75 cm in the China seas (Fig. 7b). On average, the MRSL rise under RCP8.5 (Fig. 7b) is about 18 cm higher than that under RCP4.5 (Fig. 7a) in the study region. The above projections are essentially the same as the IPCC AR5 results (Church et al., 2013).

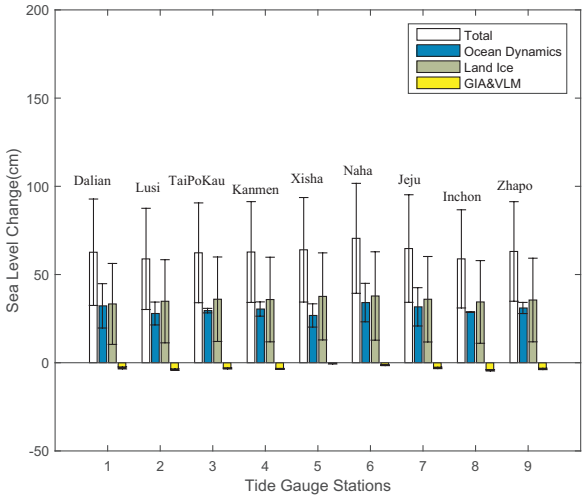

Fig. 8. Projected total MRSL changes and associated uncertainty (± one standard error) between 1986–2005 and 2081–2100 under RCP8.5, and the contributions by the steric and dynamic ocean adjustment (Ocean Dynamics in the Fig legend) based on 21 IPCC AR5 climate models (Slangen et al., 2014), by the land-ice melt from Slangen et al.'s (2014) land-ice model, and by the GIA from Peltier's (2004) model.

Fig. 8 shows the projected total MRSL rise at the selected tide-gauge sites (Fig. 1) between 1986–2005 and 2081–2100 under RCP8.5, and the contribution by steric and dynamic ocean adjustment based on 21 CMIP5 AOGCMs (Slangen et al., 2014), by land-ice melt from Slangen et al.'s (2014) land-ice estimates, and by the GIA effect from Peltier's (2004) model. The total MRSL rise is about 65 cm on average across the tide-gauge stations, showing relatively small spatial difference among all the sites. The steric and dynamic ocean effect is about 30 cm, not

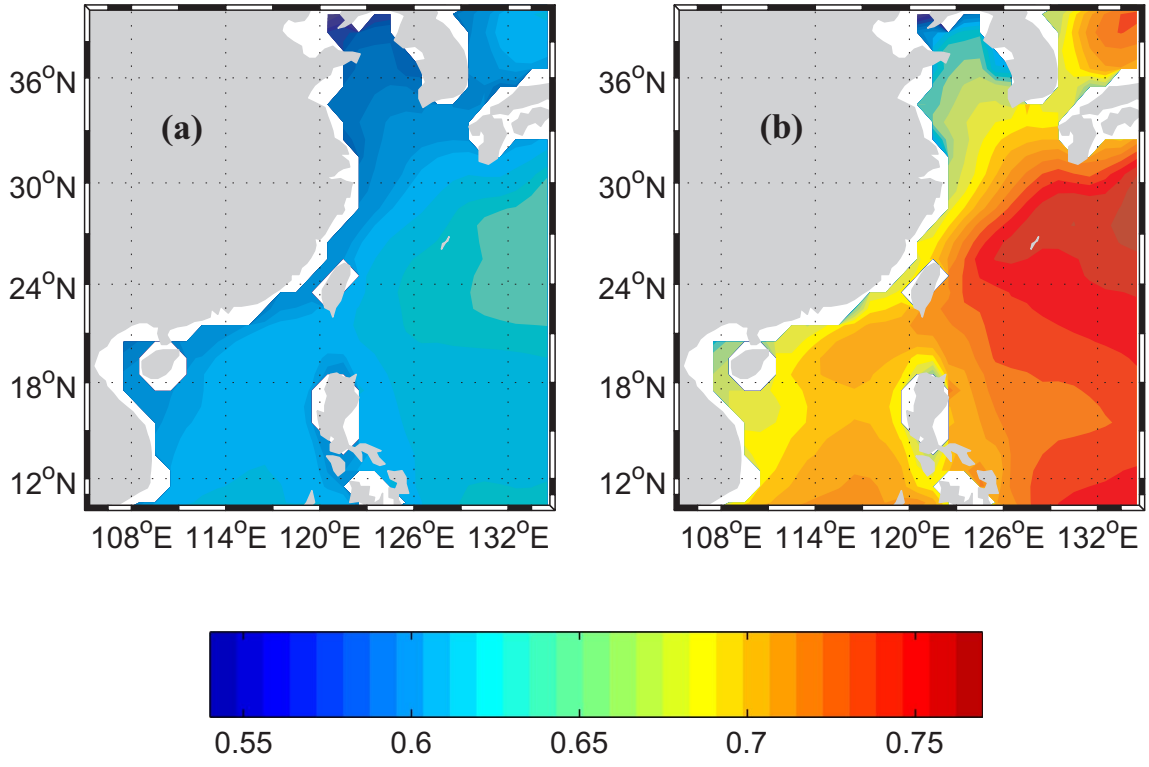

Fig. 7. Projected sea level changes (m) between 1986–2005 and 2081–2100 under (a) RCP 4.5 and (b) RCP 8.5, from Slangen et al. (2014).

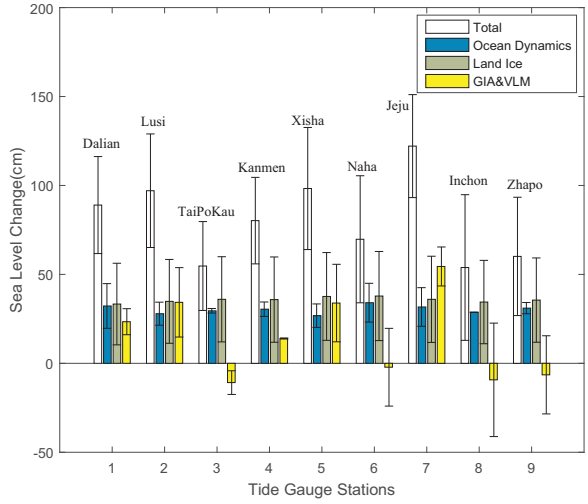

Fig. 9. Same as Fig. 8 but with the VLM from Peltier's (2004) model replaced by GPS or ATG VLM (GIA & VLM in the Fig legend).

much different from the global mean. This ocean effect is larger than Chen et al.'s (2014) projections of 12–20 cm for the Bohai and East China Seas under IPCC A2 emission scenario, which is from one single climate model only; while our results are under IPCC RCP8.5 and from the ensemble mean of 21 climate models. The fingerprint of land-ice melt contributes to the MRSL rise by about 35 cm, similar to the global mean. The Peltier's (2004) GIA contribution is negative and small.

However, when the VLM in the GIA model is replaced by the GPS or ATG-based VLM, the large land subsidence significantly augments the sea level rise at Jeju, Xisha, Lusi, Kanman and Dalian (Fig. 9 versus Fig. 8). Han et al. 2015b showed such augmentation at Jeju and at North American coastal locations. The largest rise, about 130 cm, is projected at Jeju. The total MRSL rise at all sites varies from 60 to 130 cm. The local VLM effect varies from −10 to 60 cm. As discussed in Section 3.2, the large land subsidence at sites such as Jeju and Lusi is mainly associated with local ground water extraction. As a result, the projected total MRSL rise at the tide-gauge stations varies predominately with the ATG VLM. The projected total MRSL rise under RCP4.5 shows a similar spatial variation but with smaller (by 18 cm averaged over these tide-gauge stations) amplitude (Fig. 10), due to smaller ocean and land-ice components.

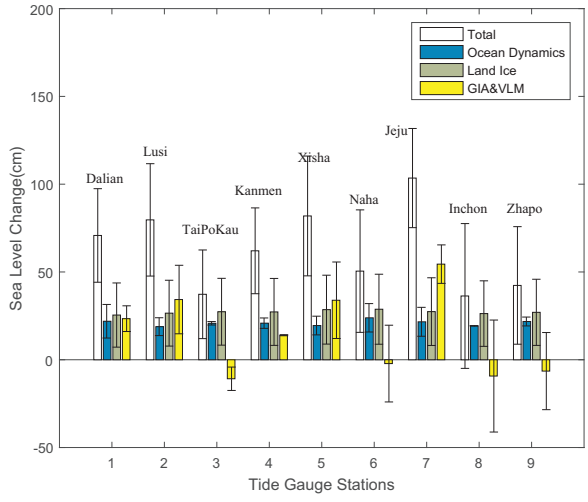

Fig. 10. Same as Fig. 9 but under RCP4.5.

5. Discussions

The preset study shows that the GIA model VLM is unable to explain the large spatial difference in the coastal MRSL in the China Seas in the past half century or so. In addition, by using the GIA model VLM, the MRSL projections in the 21st century do not vary much across the tide-gauge stations in the China Seas, as shown by well publicized literature (Church et al., 2013; Slangen et al., 2014). In contrast, the GPS VLM and ATG VLM have large spatial difference across the tide-gauge stations in the China Seas and are consistent with past MRSL difference across these stations. By using the GPS VLM or ATG VLM, the MRSL projections in the 21st century show large spatial difference across the coastal tide gauges in the China Seas. Therefore the present study points to the large impacts of using satellite-derived VLM on projecting local MRSL.

The MRSL projections are subject to large uncertainty. The uncertainty in the total MRSL projections is the root-sum-square of that associated with each component and is mainly from the land-ice component and the ATG VLM component (Figs. 8, 9 and 10). The uncertainty associated with the ocean and land-ice components represents the RMS spread of projections from process-based models (Slangen et al., 2014). The uncertainty associated with GIA represents the absolute difference of two GIA models (Slangen et al., 2014). The uncertainty associated with the ATG VLM does not explicitly account for the extrapolation and grid resolution effects of the altimetric data. Nevertheless, we have carried out an independent evaluation of the ATG VLM against the GPS VLM in Section 3.2 and Table 2. The mean bias of −0.8 mm/yr (relative to the GPS VLM) in the ATG VLM is equivalent to an MRSL overestimation of 8 cm over the projection period. The RMS difference of 1.0 mm/yr is equivalent to an MRSL uncertainty of 10 cm over the projection period. The bias and uncertainty are much less than the spatial difference of 70 cm in the ATG VLM contribution.

Since the ATG VLM compared with the GPS VLM can cause a mean bias (overestimation) of 8 cm and an RMS uncertainty of 10 cm over the projection period, GPS VLMs should be used, where possible, to replace ATG VLMs in the projection. A caveat is that GPS records available may not be long enough and therefore might not capture long-term VLM well. We recommend more long-term GPS stations be installed at tide gauge locations and existing GPS data be made available to the scientific community.

A key assumption in the MRSL projection in this study is that the VLM rate in the projection period will be the same as that at the present. Unlike the GIA effect, some of the VLM components such as due to ground water extraction, sediment compaction, and tectonic movement may vary significantly during the projection period. Because of the large contribution of the VLM component in the study region, it is necessary to revise projections if a substantial change in the VLM rate occurs or as new information on these VLM components is available. The present study also points to the need to develop models that can project VLMs associated with various processes at local scales. Until then, assuming the observed historical trends to continue offers the arguably best feasible approach.

6. Conclusions

We have used tide gauge and satellite altimetry data to investigate historical MRSL trends and then combined the contributions that account for ocean-atmosphere interactions (from global climate models), GIA (from model), land-ice melt (from model) and non-GIA VLM (from GPS or ATG) to generate MRSL rise projections for selected tide-gauge stations in the China Seas.

The past MRSL change at the tide-gauge stations in the China Seas shows significant regional variations, from 1 to 5 mm/yr, substantially different from the global mean sea level rise (Church and White, 2011). The spatial differences in the past MRSL trends are mainly associated

with that in VLM. The ATG estimates for VLM are largely negative. They are significantly different from the GIA model output, suggesting other important factors such as local ground water extraction and sediment compaction causing the VLM.

The projected MRSL rise between 1986–2005 and 2081–2100 under RCP8.5, adjusted for the GPS- or ATG-estimated VLM varies from 60 to130 cm among the tide-gauge sites. Therefore the projected sea level changes at some of the sites are substantially greater than both the global means and regional projections by IPCC AR5 (Church et al., 2013) and Slangen et al. (2014). The difference is mainly a result of accounting for VLM derived from satellite observations in the present study. The VLM effect varies from −10 to 60 cm. The steric and dynamic ocean effect and the fingerprint of the land-ice (glaciers and ice sheets) melt are comparable (about 30 cm each). The ocean effect and the land-ice melt effect do not change much spatially in the study region or differ much from the global mean. The projections under the RCP4.5 scenario show a similar spatial pattern to those under RCP8.5, with a smaller amount of rise by 18 cm on average for this region.

Acknowledgments

Tide-gauge data are obtained from the PSMSL, UK (http://www.psmsl.org/). The altimeter data are from AVISO, France (http://www.aviso.oceanobs.com/en/altimetry/index.html). GH thanks Aimee Slangen for providing global model output of the steric and dynamic ocean effect and of the land-ice melt effect. This work is partially supported by the Global Change and Air Sea Interaction Program of China: GASI-IPOVAI-04, the National 863 Program of China [No. 2013AA09A505], the National Natural Science Foundation of China [Grant No. 41321004], and the National Basic Research Programme of China [2013CB430302]. Helpful comments and suggestions were received from two anonymous reviewers.

References

Bouin, M., Woppelmann, G., 2010. Land motion estimates from GPS at tide gauges: a geophysical evaluation. Geophys. J. Int. 180 (1), 193–209. http://dx.doi.org/10.1111/j.1365-246x.2009.04411.x.

Carton, J., Giese, B., 2008. A reanalysis of ocean climate using simple ocean data assimilation (SODA). Mon. Weather Rev. 136 (8), 2999–3017. http://dx.doi.org/10.1175/2007mwr1978.1.

Cazenave, A., 2004. Present-day sea level change: observations and causes. Rev. Geophys. 42 (3). http://dx.doi.org/10.1029/2003rg000139.

Chang, C., Hsu, H., Wu, C., Sheu, W., 2008. Interannual mode of sea level in the South China Sea and the roles of El Niño and El Niño Modoki. Geophys. Res. Lett. 35 (3). http://dx.doi.org/10.1029/2007gl032562.

Chen, C.-L., Zuo, J.-C., Chen, M.-X., Gao, Z.-G., Shum, C.-K., 2014. Sea level change under IPCC-A2 scenario in Bohai, yellow, and East China Seas. Water Sci. Eng. 7 (4), 446–456.

Chen, Q., Liu, G., Ding, X., Hu, J., Yuan, L., Zhong POmura, M., 2010. Tight integration of GPS observations and persistent scatterer InSAR for detecting vertical ground motion in Hong Kong. Int. J. Appl. Earth Obs. Geoinf. 12 (6), 477–486. http://dx.doi.org/10.1016/j.jag.2010.05.002.

Cheng, X., Xie, S.-P., Du, Y., Wang, J., Chen, X., Wang, J., 2016a. Interannual-to-decadal variability and trends of sea level in the South China Sea. Clim. Dyn. 46 (9–10), 3113–3126.

Cheng, Y., Plag, H.-P., Hamlington, B., Xu, Q., He, Y., 2015. Regional sea level variability in the Bohai Sea, Yellow Sea, and East China Sea. Cont. Shelf Res. 111, 95–107.

Cheng, Y., Hamlington, B., Plag, H.-P., Xu, Q., 2016b. Influence of ENSO on the variation of annual sea level cycle in the South China Sea. Ocean Eng. 126, 343–352. http://dx.doi.org/10.1016/j.oceaneng.2016.09.019.

Choi, H., 2012. Changes of groundwater conditions on Jeju volcanic island, Korea: implications for sustainable agriculture. Afr. J. Agric. Res. 7 (4). http://dx.doi.org/10.5897/ajarx11.078.

Cheng, X., Qi, Y., 2007. Trends of sea level variations in the South China Sea from merged altimetry data. Glob. Planet. Change 57 (3–4), 371–382. http://dx.doi.org/10.1016/j.gloplacha.2007.01.005.

Church, J., White, N., 2011. Sea-Level Rise from the Late 19th to the Early 21st Century. Surv. Geophys. 32 (4–5), 585–602. http://dx.doi.org/10.1007/s10712-011-9119-1.

Church, J., Clark, P., Cazenave, A., Gregory, J., Jevrejeva, S., Levermann, A., Merrifield, M., Milne, G., Nerem, R., Nunn, P., Payne, A., Pfeffer, W., Stammer, Unnikrishnan, A., 2013. Sea level change. In: Stocker, T., Qin, D., Plattner, G., Tignor, M., Allen, S., Boschung, J., Nauels, A., Xia, Y., Bex, V., Midgley, P. (Eds.), Climate Change 2013: The Physical Science Basis. Contribution of Working Group I to the FifthAssessment Report of the Intergovernmental Panel on Climate Change. Cambridge University Press, Cambridge, United Kingdom and New York, NY, USA.

Durbin, J., Watson, G., 1950. Testing for serial correlation in least squares regression. I. Biometrika 37, 409–428.

Fang, G., Chen, H., Wei, Z., Wang, Y., Wang, X., Li, C., 2006. Trends and interannual variability of the South China Sea surface winds, surface height, and surface temperature in the recent decade. J. Geophys. Res. 111 (C11). http://dx.doi.org/10.1029/2005jc003276.

Feng, X., Tsimplis, M., Woodworth, P., 2015. Nodal variations and long-term changes in the main tides on the coasts of China. J. Geophys. Res.: Oceans 120 (2), 1215–1232. http://dx.doi.org/10.1002/2014jc010312.

Fu, L., Cazenave, A. (Eds.), 2001. Satellite Altimetry and Earth Sciences, A Handbook of Technique and Applications. Academic Press, pp. 463.

Han, G., Ikeda, M., Smith, P., 1993. Annual variation of sea-surface slopes over the Scotian Shelf and Grand Banks from Geosat altimetry. Atmos. -Ocean 31 (4), 591–615. http://dx.doi.org/10.1080/07055900.1993.9649487.

Han, G., Ma, Z., Bao, H., Slangen, A., 2014. Regional differences of relative sea level changes in the Northwest Atlantic: historical trends and future projections. J. Geophys. Res.: Oceans 119 (1), 156–164. http://dx.doi.org/10.1002/2013jc009454.

Han, G., Ma, Z., Chen, N., Thomson, R., Slangen, A., 2015a. Changes in mean relative sea level around canada in the twentieth and twenty-first centuries. Atmos. -Ocean 53 (5), 452–463. http://dx.doi.org/10.1080/07055900.2015.1057100.

Han, G., Ma, Z., Chen, N., Yang, J., Chen, N., 2015b. Coastal sea level projections with improved accounting for vertical land motion. Sci. Rep. 5 (1). http://dx.doi.org/10.1038/srep16085.

Han, G., Huang, W., 2008. Pacific Decadal Oscillation and Sea Level Variability in the Bohai, Yellow, and East China Seas. J. Phys. Oceanogr. 38 (12), 2772–2783. http://dx.doi.org/10.1175/2008jpo3885.1.

Han, G., Huang, W., 2009. Low-frequency sea-level variability in the South China Sea and its relationship with ENSO. Theor. Appl. Climatol. 97 (3–4). http://dx.doi.org/10.1007/s00704-009-0116-y. (403-403).

Hay, C., Morrow, E., Kopp, R., Mitrovica, J., 2015. Probabilistic reanalysis of twentieth-century sea-level rise. Nature 517 (7535), 481–484. http://dx.doi.org/10.1038/nature14093.

Lambeck, K., Smither, C., Ekman, M., 1998. Tests of glacial rebound models for Fennoscandinavia based on instrumented sea- and lake-level records. Geophys. J. Int. 135 (2), 375–387. http://dx.doi.org/10.1046/j.1365-246x.1998.00643.x.

Lena, P., 2012. The influence of air pressure and atmospheric circulation on sea level variability in China (Master of Science Thesis). University of Gothenberg, Sweden.

Liu, S., 2013. Kanmen tide-gauge station. Zhejiang Arch. http://dx.doi.org/10.3969/j.issn.1006-4176.2013.10.021. (in Chinese).

Moss, R., Edmonds, J., Hibbard, K., Manning, M., Rose, S., van Vuuren, D., Carter, T., Emori, S., Kainuma, M., Kram, T., Meehl, G., Mitchell, J., Nakicenovic, N., Riahi, K., Smith, S., Stouffer, R., Thomson, A., Weyant, J., Wilbanks, T., 2010. The next generation of scenarios for climate change research and assessment. Nature 463 (7282), 747–756. http://dx.doi.org/10.1038/nature08823.

Nerem, R., Chambers, D., Choe, C., Mitchum, G., 2010. Estimating mean sea level change from the TOPEX and Jason Altimeter Missions. Mar. Geod. 33 (Suppl 1), S435–S446. http://dx.doi.org/10.1080/01490419.2010.491031.

Peltier, W., 2004. Global glacial isostasy and the surface of the ice-age earth: the ICE-5G (VM2) model and grace. Annu. Rev. Earth Planet. Sci. 32 (1), 111–149. http://dx.doi.org/10.1146/annurev.earth.32.082503.144359.

Ren, M., 1994. Relative sea level changes in China over the last 80 years. In: Oceanology of China Seas. Springer, pp. 433–444.

Rong, Z., Liu, Y., Zong, H., Cheng, Y., 2007. Interannual sea level variability in the South China Sea and its response to ENSO. Glob. Planet. Change 55 (4), 257–272. http://dx.doi.org/10.1016/j.gloplacha.2006.08.001.

Sallenger, A., Doran, K., Howd, P., 2012. Hotspot of accelerated sea-level rise on the Atlantic coast of North America. Nat. Clim. Change 2 (12), 884–888. http://dx.doi.org/10.1038/nclimate1597.

Slangen, A., Carson, M., Katsman, C., van de Wal, R., Köhl, A., Vermeersen, L., Stammer, D., 2014. Projecting twenty-first century regional sea-level changes. Clim. Change 124 (1–2), 317–332. http://dx.doi.org/10.1007/s10584-014-1080-9.

Slangen, A., Katsman, C., van de Wal, R., Vermeersen, L., Riva, R., 2012. Towards regional projections of twenty-first century sea-level change based on IPCC SRES scenarios. Clim. Dyn. 38 (5–6), 1191–1209. http://dx.doi.org/10.1007/s00382-011-1057-6.

Strassburg, M., Hamlington, B., Leben, R., Manurung, P., Lumban Gaol, J., Nababan, B., Vignudelli, S., Kim, K.-Y., 2015. Sea level trends in Southeast Asian seas. Clim. Past 11 (5), 743–750.

Su, J., Yuan, Y. (Eds.), 2005. Hydrography in the Chinese Seas. Ocean Press, Beijing, pp. 367 (in Chinese).

Taylor, K., Stouffer, R., Meehl, G., 2012. An overview of CMIP5 and the experiment design. Bull. Am. Meteorol. Soc. 93 (4), 485–498. http://dx.doi.org/10.1175/bams-d-11-00094.1.

UNESCO/ICO, 2010. Sea-Level Rise and Variability – A Summary for Policy Makers. IOC/BRO/2010/5, France.

Vignudelli, S., Kostianoy, A., Cipollini, P., Benveniste, J. (Eds.), 2011. Coastal Altimetry. Springer-Verlag, pp. 565.

Watson, C., White, N., Church, J., King, M., Burgette, R., Legresy, B., 2015. Unabated global mean sea-level rise over the satellite altimeter era. Nat. Clim. Change 5 (6), 565–569.

Wöppelmann, G., Marcos, M., 2016. Vertical land motion as a key to understanding sea level change and variability. Rev. Geophys. 54 (1), 64–92. http://dx.doi.org/10.1002/2015rg000502.

Zhu, J., Yang, Y., Yu, J., Gong, X., 2015. Land subsidence of coastal areas of Jiangsu Province, China: historical review and present situation. Proc. Int. Assoc. Hydrol. Sci. 372, 503–506. http://dx.doi.org/10.5194/piahs-372-503-2015.